

Load/Source-Pull Evaluation of Modulated Performance in GaAs HBT Power Cells for WiFi-6

*Original*

Load/Source-Pull Evaluation of Modulated Performance in GaAs HBT Power Cells for WiFi-6 / Angelotti, Alberto Maria; Florian, Corrado; Gibiino, Gian Piero; Ramella, Chiara; Pirola, Marco; Manni, Francesco; Giofrè, Rocco; Colantonio, Paolo. - (2025), pp. 1-4. ( 2025 International Workshop on Integrated Nonlinear Microwave and Millimetre-Wave Circuits, INMMiC 2025 Torino (Ita) 10-11 April 2025) [10.1109/inmmic64198.2025.10975718].

*Availability:*

This version is available at: 11583/3004911 since: 2025-11-06T13:03:20Z

*Publisher:*

IEEE

*Published*

DOI:10.1109/inmmic64198.2025.10975718

*Terms of use:*

This article is made available under terms and conditions as specified in the corresponding bibliographic description in the repository

*Publisher copyright*

IEEE postprint/Author's Accepted Manuscript

©2025 IEEE. Personal use of this material is permitted. Permission from IEEE must be obtained for all other uses, in any current or future media, including reprinting/republishing this material for advertising or promotional purposes, creating new collecting works, for resale or lists, or reuse of any copyrighted component of this work in other works.

(Article begins on next page)

# Load/Source-Pull Evaluation of Modulated Performance in GaAs HBT Power Cells for WiFi-6

Alberto Maria Angelotti  
*Università di Bologna, DEI*  
 Bologna, Italy  
 0000-0003-2088-9663

Corrado Florian  
*Università di Bologna, DEI*  
 Bologna, Italy  
 0000-0002-5652-9355

Gian Piero Gibiino  
*Università di Bologna, DEI*  
 Bologna, Italy  
 0000-0002-1261-9527

Chiara Ramella  
*Politecnico di Torino, DET*  
 Torino, Italy  
 0000-0003-0634-1474

Marco Pirola  
*Politecnico di Torino, DET*  
 Torino, Italy  
 0000-0002-5759-9697

Francesco Manni  
*Univ. di Roma Tor Vergata, DIE*  
 Roma, Italy  
 0009-0005-1503-9455

Rocco Giofrè  
*Univ. di Roma Tor Vergata, DIE*  
 Roma, Italy  
 0000-0002-7503-0373

Paolo Colantonio  
*Univ. di Roma Tor Vergata, DIE*  
 Roma, Italy  
 0000-0002-5788-1262

**Abstract**—This work establishes a methodology based on continuous-wave load-pull data in order to estimate modulated figures of merit for radio-frequency transistors. By automatically accounting for source termination effects without any measurement overhead, the technique allows to fully explore the intrinsic trade-offs between linearity, gain, output power and power added efficiency. The approach is used to experimentally analyze three different layouts of gallium arsenide (GaAs) Heterojunction Bipolar Transistor (HBT) power cells for Wi-Fi 6 applications.

**Index Terms**—Microwave measurement, HBT, GaAs, WiFi-6

## I. INTRODUCTION

The last generation of wireless networking standards (WiFi 6, 802.11ax), while delivering unprecedented performance in terms of communication speed [1], imposes challenging requirements for power amplifiers (PAs) within the transmission signal chain. The adopted Orthogonal Frequency Division Multiplexing (OFDM) modulation schemes result in time-domain waveforms with peak-to-average power ratios (PAPR) in excess of 10 dB, for which specific techniques are required to obtain high-efficiency and linear PAs, particularly in the case of dense constellations [2]. These conflicting demands have to be addressed at all stages during the design process, where critical optimizations can be implemented already at transistor level [3].

In this work, three custom gallium arsenide (GaAs) Heterojunction Bipolar Transistor (HBT) power cells, implemented in the H20U-C4 process from WIN Semiconductors, are experimentally analyzed to evaluate their suitability for the realization of WiFi-6 PAs. A methodology is proposed to assess the cells' performance in the final circuit when excited with application-like modulated test signals [4], providing a comprehensive evaluation of their linearity and efficiency. Using standard continuous wave (CW) load-pull (LP) data, multiple relevant source and load impedances are tested, allowing to explore trade-offs between linearity, output power, gain, and power added efficiency (PAE), and highlighting the relative advantages of each design.

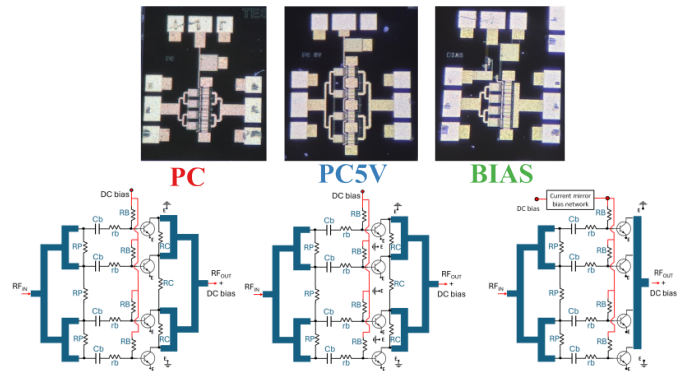


Fig. 1. Photographs and schematics of the three power cells.

## II. DESIGN OF THE HBT POWER CELLS

The photographs of the power cells (referred as "PC", "PC5V" and "BIAS", respectively) and the corresponding schematics are shown in Fig. 1. The cells are implemented by combining four 4-finger  $3 \times 40 \mu\text{m}^2$  HBT fingers, for a total active periphery of  $1920 \mu\text{m}^2$ , with expected  $\sim 30$  dBm of saturated output power in the 5-7 GHz frequency range. DC base ballast resistors ( $R_B$ ) are used to ensure thermal stability of the power cells, while RF ballasting and feedback is implemented with  $r_b$  and  $C_b$ . All cells include odd-mode stabilization resistances ( $R_P$  and  $R_C$ ). With respect to the standard combined structure in PC, PC5V adds additional ground vias to reduce the effect of source inductances. The BIAS cell, instead, modifies the output combiner structure and includes an additional current mirror bias circuit in the base.

## III. LOAD-PULL-BASED EVALUATION METHODOLOGY

Each voltage-biased transistor device-under-test (DUT) is modeled as a quasi-static time-invariant nonlinear 2-port circuit terminated with a linear passive load  $\Gamma_L$ , as depicted

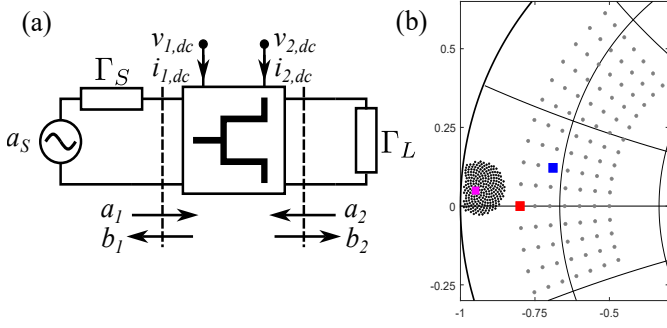


Fig. 2. (a) Schematic of a general LP experimental setup. (b) Smith chart plot for the  $\Gamma_S$ -grid (black),  $\Gamma_S = -0.95 + j0.05$  (magenta), the  $\Gamma_L$  grid (grey), the maximum PAE load ( $\Gamma_L = -0.69 + j0.12$ , blue), the maximum  $P_{out}$  load ( $\Gamma_L = -0.8$ , red) in CW LP for the PC5V cell at 6 GHz.

in Fig. 2a. In this way, neglecting harmonic components and terminations, the constitutive equations read

$$\begin{aligned} b_1 &= f_1(|a_1|, \Gamma_L) a_1 & b_2 &= f_2(|a_1|, \Gamma_L) a_1 \\ i_{1,dc} &= g_1(|a_1|, \Gamma_L) & i_{2,dc} &= g_2(|a_1|, \Gamma_L) \end{aligned} \quad (1)$$

where  $a_k$ ,  $b_k$  are the incident and reflected power waves at the fundamental frequency, and  $i_{k,dc}$  is the dc component of the current, each respectively at each at port  $k = 1, 2$  [5]. The functions in (1) are typically extracted from vector LP experiments, where the magnitude of  $a_1$  and  $\Gamma_L$  are swept independently to capture all the variables needed to provide the relevant figures-of-merit (FoMs) for the DUT. This test is often performed using a source generator with a 50- $\Omega$  impedance ( $\Gamma_S = 0$ ), as the source impedance does not appear in any form in (1) and, therefore, does not impact most of the relevant metrics of interest for the DUT.

Results for any source termination  $\Gamma_S \neq 0$  do not require additional measurements and can be obtained by suitably post-processing the standard LP data [6]. In general, any linear source can be represented as

$$a_1 = a_S + \Gamma_S b_1 \implies a_S = a_1 - \Gamma_S f_1(|a_1|, \Gamma_L). \quad (2)$$

The  $a_1$ ,  $b_1$  and  $\Gamma_L$  values known from a LP experiment at  $\Gamma_S = 0$  can be used in (2) to derive the “virtual” excitation  $a_S$  that would result in the exact same DUT waves, for any user-prescribed  $\Gamma_S \neq 0$ . Moreover, (2) can be inverted to provide  $a_1$  as a function of  $a_S$ ,  $\Gamma_S$  and  $\Gamma_L$ :  $a_1 = h(|a_S|, \Gamma_S, \Gamma_L) a_S$ , which can then be substituted in (1) to obtain all the other waves. This elaboration strategy allows to derive the behavior of the DUT for general  $\Gamma_S$ - $\Gamma_L$  terminations, such as those imposed by the matching network of the final PA. The following FoMs can then be defined:

$$\begin{aligned} P_{av,S} &= \frac{|a_S|^2}{2(1 - |\Gamma_S|^2)} & P_{out} &= \frac{1}{2}|b_2|^2 - \frac{1}{2}|a_2|^2 \\ G_T &= \frac{P_{out}}{P_{av,S}} & PAE &= \frac{P_{out} - P_{av,S}}{v_{1,dc}i_{1,dc} + v_{2,dc}i_{2,dc}}. \end{aligned} \quad (3)$$

The post-processing of LP data by assuming a specific  $\Gamma_S$  is necessary for the correct evaluation of linearity, which is

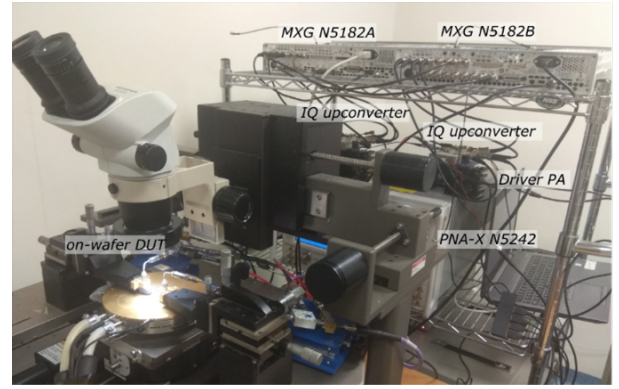


Fig. 3. The on-wafer active load-pull measurement setup used in this work.

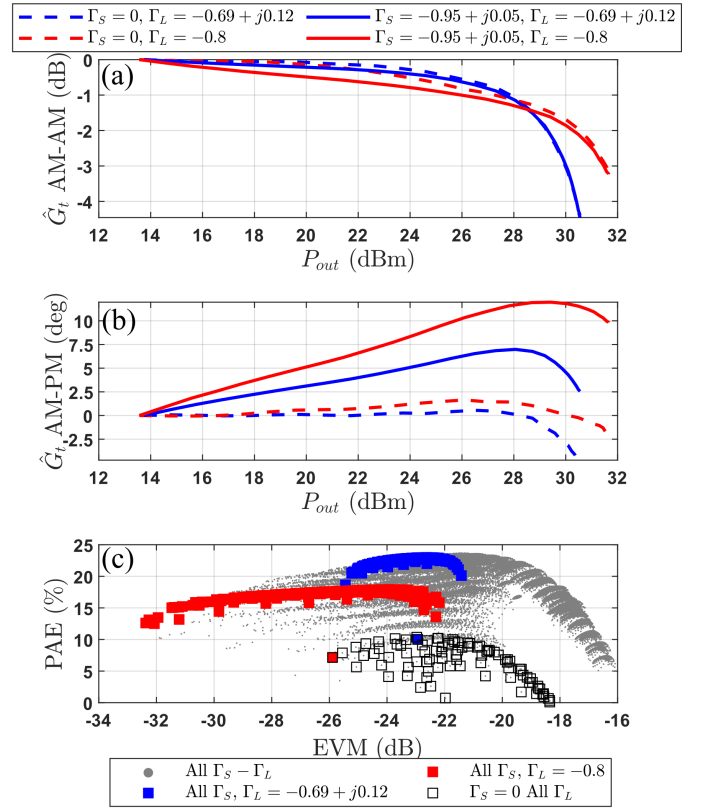


Fig. 4. (a) AM-AM and (b) AM-PM characteristics for the CW complex transducer gain  $\hat{G}_T$  of the PC5V cell for  $\Gamma_S = -0.95 + j0.05$  (line) and  $\Gamma_S = 0$  (dash) and the maximum PAE  $\Gamma_L$  (blue) and maximum  $P_{out}$   $\Gamma_L$  (red). (c) Modulated PAE and EVM results for the PC5V transistors for all the examined  $\Gamma_S - \Gamma_L$  combinations (grey), for the maximum PAE  $\Gamma_L$  (blue), for the maximum  $P_{out}$   $\Gamma_L$  (red) and for  $\Gamma_S = 0$  (black squares).

strongly dependent on the input termination [6]. The nonlinear distortion introduced by the DUT within the final circuit is computed on the observed output  $b_2$  (or equivalently  $a_2$ ) for a given input  $a_S$ . This can be quantified using the AM-AM and AM-PM characteristics of the DUT complex transducer gain  $\hat{G}_T = \frac{b_2}{a_S}$  for specific  $\Gamma_S$ - $\Gamma_L$  conditions [6], which are generally different from the distortion between the  $b_2$ - and  $a_1$ -waves, due to the nonlinearity in (2).

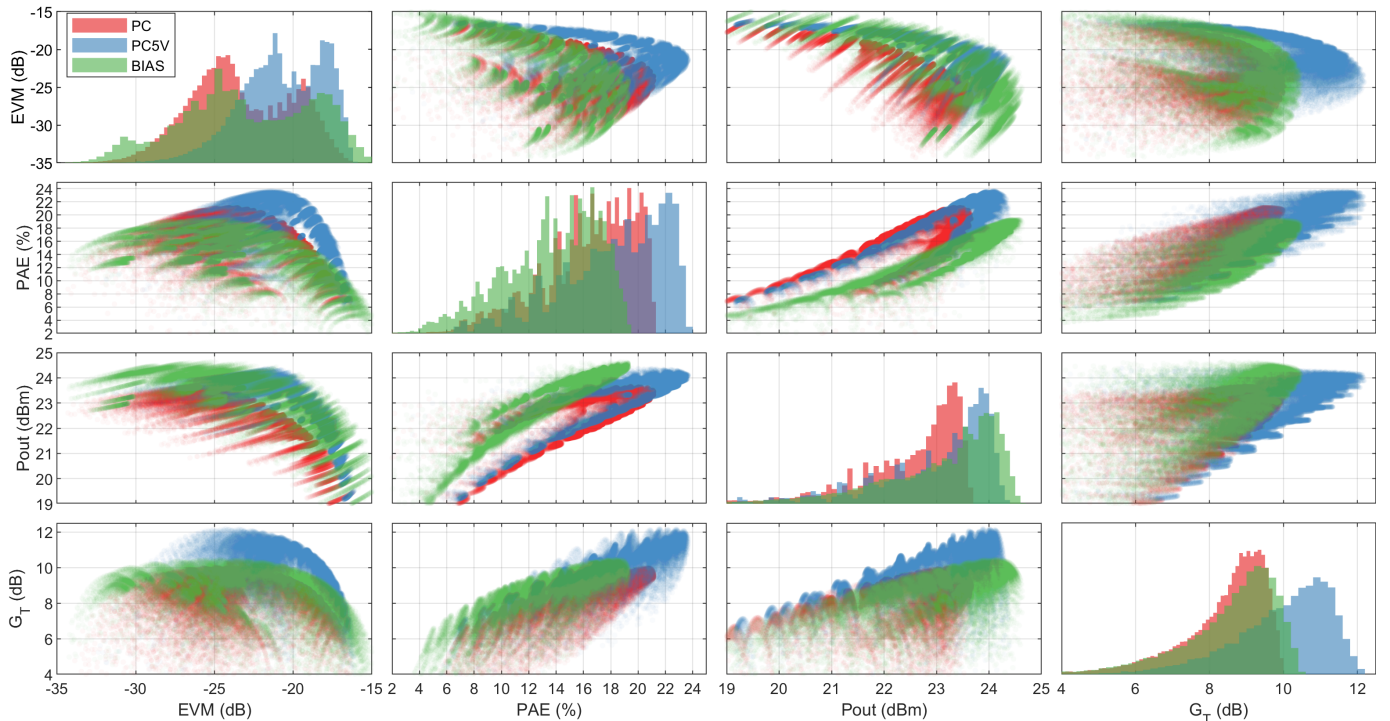


Fig. 5. Scatter matrix plots for the PC (red), PC5V (blue) and BIAS (green) cells for the EVM-PAE-Pout-GT trade-offs. Each data point represents, for a given  $\Gamma_S$ - $\Gamma_L$  choice, the value of the respective metric for the DUT excited by a full-swing random-phase multi-sine with PAPR=10.1 dB. The X-Y intersection plots represent the metric X as a function of metric Y, while X-X plots on the diagonal represent the overall distribution of the values of variable X.

The CW operating characteristics in a specific  $\Gamma_S$ - $\Gamma_L$  environment can also be used to estimate FoMs in modulated conditions by superimposing a specific modulated signal to  $a_S$  and by examining the resulting envelopes for the variables in (1) [4], [7]. The use of this quasi-stationary approach neglects any memory effect in DUT, but avoids the use of a significantly more complex wideband setup for characterization [4]. In this case, the FoMs in (3) are derived as suitable statistical or time-averages of the corresponding CW quantities. Moreover, all the linearity FoMs dictated by the waveform standards can be directly computed. For example, EVM can be derived as [4], [7]

$$\text{EVM} = \frac{\int |b_2(t) - G \cdot a_S(t)|^2 dt}{\int |b_2(t)|^2 dt}, \quad (4)$$

where  $G$  is the statistical average of the DUT complex transducer gain. While different input signal levels can be tested to examine performance in back-off conditions, in this work we derive each modulated FoM at “full-scale”, where the peak of the  $a_S(t)$  waveform corresponds to the peak power at which the CW LP data is derived.

This methodology allows to directly map CW load-pull measurements into application-relevant modulated metrics for a given transistor, allowing for a thorough evaluation of different solutions across all the possible  $\Gamma_S - \Gamma_L$  choices.

#### IV. EXPERIMENTAL RESULTS

For the three cells, a fundamental-only LP characterization is performed at a frequency of 6 GHz using the on-wafer active

setup reported in [4] and shown in Fig. 3. The quiescent point is selected as  $V_C = 5$  V and  $J_C = 10$  kA/cm<sup>2</sup> and the DUTs are kept at a fixed baseplate temperature  $T_b = 30$  °C. The load grid for the LP measurements and the source grid used for the data post-processing are reported in Fig. 2b, along with the maximum  $P_{out}$  and PAE loads for the PC5V cell. The modulated signal used as excitation is a full-swing  $10^4$ -tones multi-sine with PAPR = 10.1 dB, which can be considered as a suitable approximation for other complex-gaussian envelopes such as Wi-Fi 6 OFDM waveforms [1], [4].

Figures 4a-b report the CW  $\hat{G}_T$  AM-AM and AM-PM curves for the PC5V cell for selected values of  $\Gamma_S$  (maximum Pout and maximum PAE in CW conditions) and  $\Gamma_S$  (0 and  $\Gamma_S = -0.95 + j0.05$ ), highlighting how the source termination strongly impacts the overall circuit linearity, particularly regarding the phase distortion characteristics. PAE and EVM for the same device in modulated conditions are reported in Fig. 4c for all the tested  $\Gamma_S - \Gamma_L$  combinations. The use of synthetic modulated conditions for the DUT allows to better reflect the device achievable performance in the final application. For example, it can be observed how the maximum CW PAE  $\Gamma_L$  is not the one providing the maximum PAE in modulated operation due to the back-offed conditions, while also featuring a sub-optimal PAE-EVM trade-off with respect to the whole ensemble. A multi-dimensional scatter plot is reported in Fig. 5, comparing the  $G_T$ - $P_{out}$ -PAE-EVM trade-offs among the three cells. The PC5V cell is able to provide the highest overall gain ( $\sim 12$  dB) and PAE ( $\sim 23\%$ )

in modulated conditions, while the BIAS cell provides the highest output power ( $\sim 24.5$  dBm). It can also be observed from the PAE-vs-EVM data how the PC5V cell offers the best linearity-efficiency trade-off at high EVM values ( $> -25$  dB), the PC cell at intermediate ones ( $< -25$  dB and  $> -30$  dB), and the BIAS cell for low ones ( $< -30$  dB).

## V. CONCLUSIONS

A methodology based on source termination post-processed CW LP data has been used to evaluate the expected performance in modulated condition of three HBT cells for Wi-Fi 6 applications in the 6 GHz band. The technique allows to thoroughly analyze how the trade-offs between EVM, output power, gain and PAE are affected by the different examined topologies.

## REFERENCES

- [1] D. Lopez-Perez, A. Garcia-Rodriguez, L. Galati-Giordano, M. Kasslin, and K. Doppler, "IEEE 802.11 be extremely high throughput: The next generation of Wi-Fi technology beyond 802.11 ax," *IEEE Communications Magazine*, vol. 57, no. 9, pp. 113–119, 2019.
- [2] S. Hwang, J. Jeon, S. Bae, B. Yoon, S. Kang, and J. Kim, "A 5.15–7.125-ghz differential power amplifier with enhanced linearity of average power region using dynamic cross-coupled capacitor," *IEEE Transactions on Microwave Theory and Techniques*, vol. 72, no. 1, pp. 575–588, 2023.
- [3] A. Balasubramaniyan, X. Hui, A. Bellaouar, M. M. Campos, A. Bharamwaj, E. Veeramani, and S. Syed, "A 22FDX@ Wi-Fi PA Demonstrating a New LDMOS Device with 10V Breakdown Achieving Output Power of 29.5 dBm at 40% PAE," in *2024 IEEE Radio Frequency Integrated Circuits Symposium (RFIC)*. IEEE, 2024, pp. 35–38.
- [4] A. M. Angelotti, G. P. Gibiino, T. S. Nielsen, A. Santarelli, and J. Verspecht, "Impact of broadband modulation in active load-pull on-wafer measurements of gan hemts," in *2022 99th ARFTG Microwave Measurement Conference (ARFTG)*. IEEE, 2022, pp. 1–4.
- [5] G. P. Gibiino, A. M. Angelotti, A. Santarelli, F. Filicori, and P. A. Traverso, "Multitone multiharmonic scattering parameters for the characterization of nonlinear networks," *IEEE Trans. Instrum. Meas.*, vol. 70, pp. 1–12, 2020.
- [6] F. Vanaverbeke, L. Zhang, D. Holmes, M. Marchetti, and K. Kim, "Demystifying AM-PM characteristics through the definition of the complex Transducer Gain  $\hat{G}_T$ ," in *Proc. ARFTG Microw. Meas. Conf.* IEEE, 2020, pp. 1–8.
- [7] F. M. E. Barradas, L. C. Nunes, and J. C. Pedro, "Estimation and Sensitivity of Average Efficiency of RF PAs under Modulated Signal Stimulus," in *Proc. Int. Workshop Integ. Nonlinear Microw. MM-Wave Circ.* IEEE, 2023, pp. 1–4.